Supporting Information for

Proposing Explainable Descriptors Towards Enhanced N_2 Reduction Performance on the Two-Dimensional Bismuthine Nanosheets Modified by P-block Element-based Electrocatalysts

Dengning Sun[1], Xiaokun Du[1], Jing Chen[3], Tao Ye[1], Hao Shen[1], Ruirui Wang[5], Ying Wang[4,*], Guoqiang Liu[2], Yangyang Wan[1,*], Zhongti Sun[1,2,*]

[1] *School of Materials Science and Engineering, Jiangsu University, 212013 Zhenjiang, PR China;*

[2] *Anhui Province Key Laboratory of Efficient Conversion and Solid-State Storage of Hydrogen & Electricity, Anhui University of Technology, 243002 Maanshan, PR China;*

[3] *Hebei Key Laboratory of Photoelectric Control on Surface and Interface, College of Science, Hebei University of Science and Technology, 050018 Shijiazhuang, China;*

[4] *School of Physics and Electronic Engineering, Jiangsu University, 212013 Zhenjiang, PR China;*

[5] *School of the Environment and Safety Engineering, Jiangsu University, 212013 Zhenjiang, PR China;*

Table of contents

Section 3 Tables

Section 1 Computational details

1. Density functional theory method

All the simulations have been carried out the spin-unrestricted density functional theory (DFT), implemented by the Vienna Ab-initio Simulation Package (VASP) software with projector augmented wave pseudopotential[1]. The Revised Perdew–Burke–Ernzerhof (RPBE) functional within the Generalized Gradient Approximation (GGA)[2-3] is used to describe electron exchange and correlation energies. In the calculation processes, the energy cutoff value is set to be 400 eV, and the K-grid sampling in the first Brillouin zones is 2×2×1. We may also evaluate the effect of cutoff energy with 500 eV on the adsorption energy of key intermediates and corresponding reaction energies in Table S8. The disparities of these energies are very little, less than 0.1 eV within DFT error. The 4×4 supercell bismuthine structure was used to construct the bismuthine-based system modified by *p-block* atom. The vacuum layer thickness is 15 Å to prevent the image interactions along the direction that vertical to the substrates. Additionally, the DFT-D3 correction[4] is applied to accurately evaluate the adsorption energies of intermediates in NRR. To accurately depict the solvation effect on the capture of intermediates, the implicit solvation model (VASPsol)[5] was implemented into the entire reaction processes. The total energy and residual force per atom convergence criterion is set to be 10^{-4} eV and 0.02 eV/Å, respectively. Density of state and Crystal Orbital Hamilton Populations[6] were calculated to evaluate the bonding strength of key intermediates in the electrochemical NRR process. VASPkit tool[7] was applied to the pre-process and post-process of VASP simulation including the free energy corrections and preparing input files.

For calculating the Gibbs free energy change during the NRR reaction through coupled proton-electron transfer (CPET) process, we used the computational hydrogen electrode (CHE) model proposed by Nørskov et al[8]. The Gibbs free energy change is defined as:

$$\Delta G = \Delta E + \Delta E_{ZPE} - T\Delta S + \Delta G_{pH} + \Delta G_e \#(1)$$

where ΔE is the energy difference obtained from DFT calculations, ΔE_{ZPE} and ΔS represent the changes in zero-point energy and entropy at 298.15 K, respectively, and ΔG_{pH} and ΔG_e account for the effects of pH and electrode potential, which are not considered in this study.

The formation energy of doped- and adsorbed-Bi system was calculated using the below formula:

$E_f = E_{total} - E_{Bi} - E_{dop/ads\text{-}element}$, where E_{total} and E_{Bi} are the total energy with and without the doped-/adsorbed p-block elements, $E_{dop/ads\text{-}element}$ is the chemical potential of p-block elements referring to their stable states in the bulk phase or single layer or gas phase.

To further confirm the thermodynamical stability of potential candidates, ab-initio molecular dynamics (AIMD) simulations are carried out within the canonical (NVT) ensemble at 300 and 500 K using the Nose−Hoover thermostat[9].

2. Machine learning algorithm

Scikit-learn (sklearn), a comprehensive and widely-used Python library for machine learning, provides robust tools for establishing and analyzing relationships between datasets through its extensive collection of regression algorithms and feature importance evaluation techniques. For modeling data relationships, practitioners can leverage linear regression to capture straightforward linear correlations between input features (X) and target variables (y), while employing polynomial regression with the preprocessing capabilities to handle more complex nonlinear patterns through feature transformation. The library further supports advanced regression methods like support vector machines and ensemble approaches to address diverse relationship types. Model efficacy is quantitatively assessed using metrics such as the coefficient of determination (R^2), mean squared error, and cross-validation scores, ensuring rigorous evaluation of the fitted relationships. Regarding feature importance analysis, sklearn offers multiple methodologies: tree-based algorithms inherently provide impurity-based

importance scores through their feature importance attribute, while permutation importance enable model-agnostic interpretation of feature contributions.

The SISSO (Sure Independence Screening and Sparsifying Operator) algorithm is based on compressed sensing and symbolic regression approach[10-11]. We employed SISSO to identify the determining primary features and train a large number of physically interpretable descriptors with different dimensions and complexities. DFT-calculated inputs were used as training data. Through integrating lots of user-defined primary features with a set of mathematical operators, an enormous pool of more than 10 billion potential descriptors is created iteratively. The complexity of the ML-trained descriptors (phi) is governed by the number of times the operators are used (feature spaces). Note that the overall feature space for searching descriptors of varying complexity grows exponentially with descriptor complexity. It was taken into account up to four levels (phi = 1, 2, 3, 4) in this work. For establishing the feature spaces, we utilized the set of algebraic/functional operators given in the following:

$$\hat{H}^{(m)} \equiv \{+, -, \times, \div, log, exp, exp^{(n)}(-), ^{-1}, ^{2}, ^{3}, \sqrt{}, \sqrt[3]{}, |-|\}$$

In an ideally determined subspace, the best descriptors for each complexity and dimension are acquired.

The sparsifying ℓ_0 constraint is adapted to a smaller feature subspace that has been chosen using a screening method called sure independence screening (SIS), where the size of the subspace is equal to a user-defined SIS value multiplied by the dimension of the descriptor. The SIS value is not a typical hyperparameter, and it is not easy to optimize it using a validation data set. To find the best descriptor, one should ideally search the entire feature space. However, because the computational cost of the sparsifying ℓ_0 constraint increases exponentially with the size of the searched feature space, this is not computationally feasible. Conversely, the largest computationally feasible SIS value should be chosen. The convergence of the training error served as the basis for selecting the reasonable SIS values.

Section 2 Figures

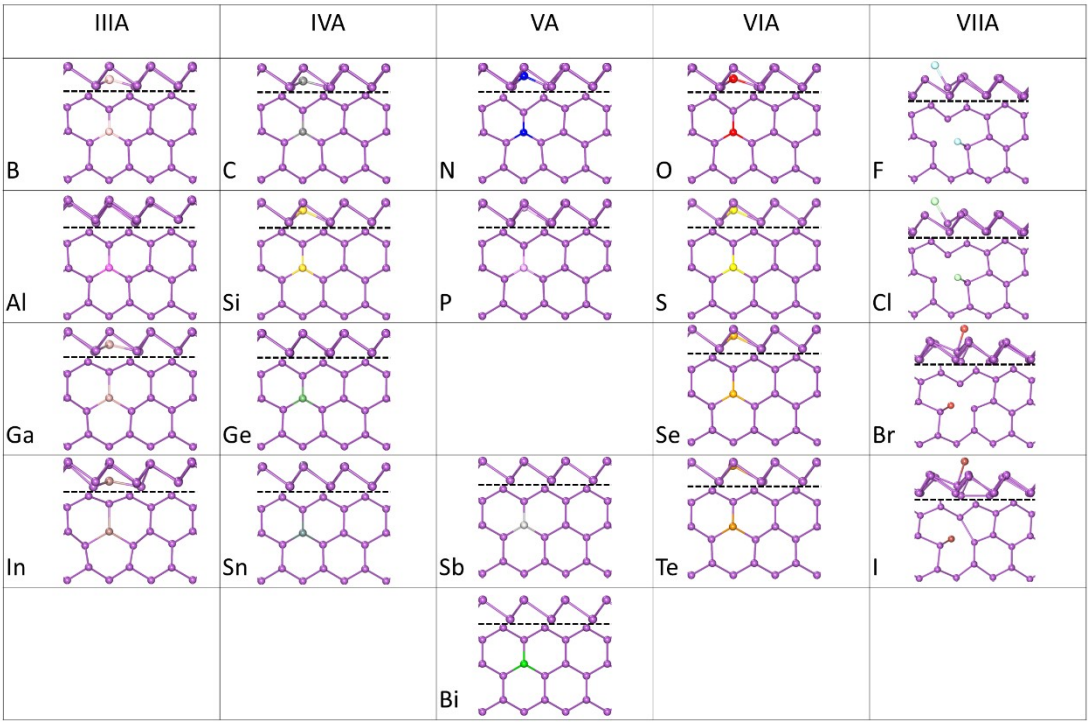

Figure S1 Optimized configurations of p-block element doped into 2D bismuthine with side (up) and top (down) view. Purple ball and other color ball indicate Bi atom and other p-block elements, respectively.

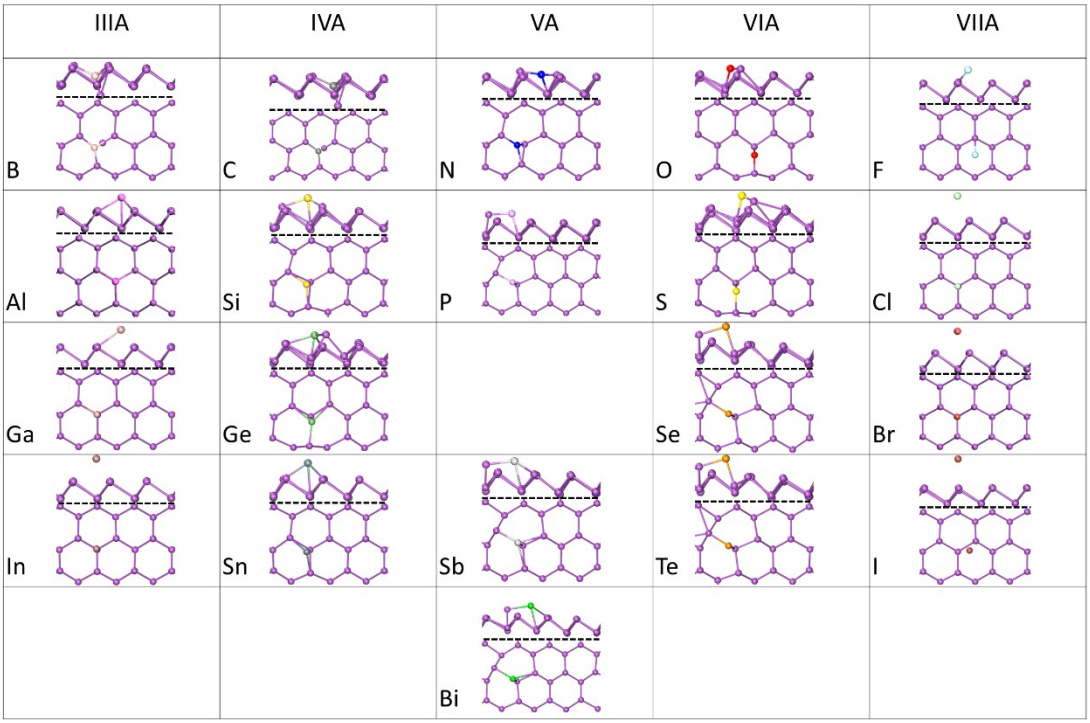

Figure S2 Optimized configurations of p-block element adsorbed onto 2D bismuthine with side (up) and top (down) view. Purple ball and other color ball indicate Bi atom and other p-block elements, respectively.

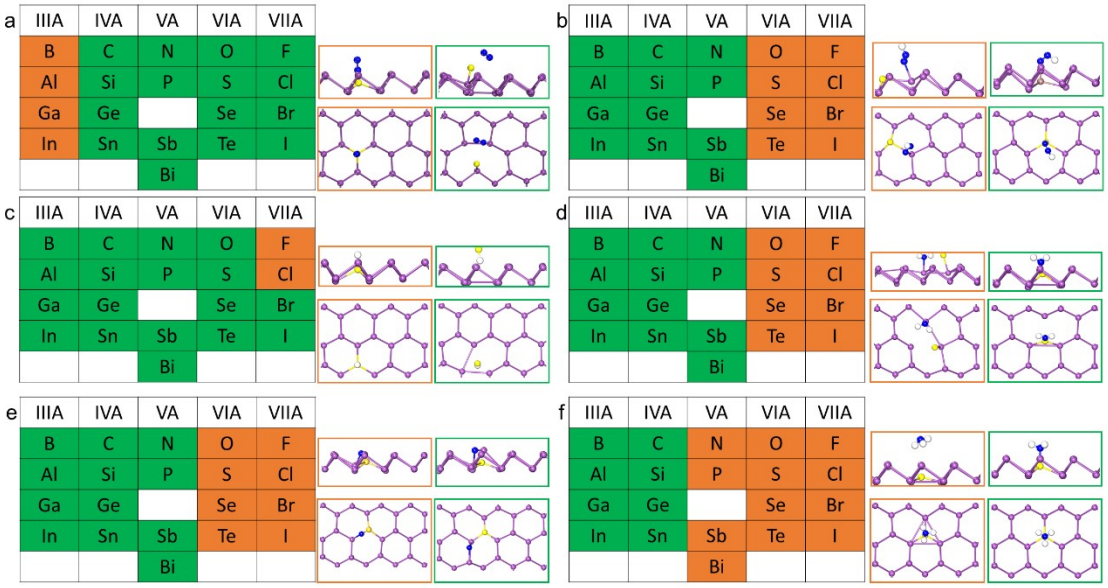

Figure S3 Optimized adsorption models of key intermediates N_2 (a), NNH (b), H (c), NH_2 (d), N (e), NH_3 (f) on the p-block element doped into bismuthine. Purple, yellow, blue, and white balls represent Bi, adsorbed p-block element, N and H atom, respectively. The orange and green colors represent the different adsorption configurations of key intermediates.

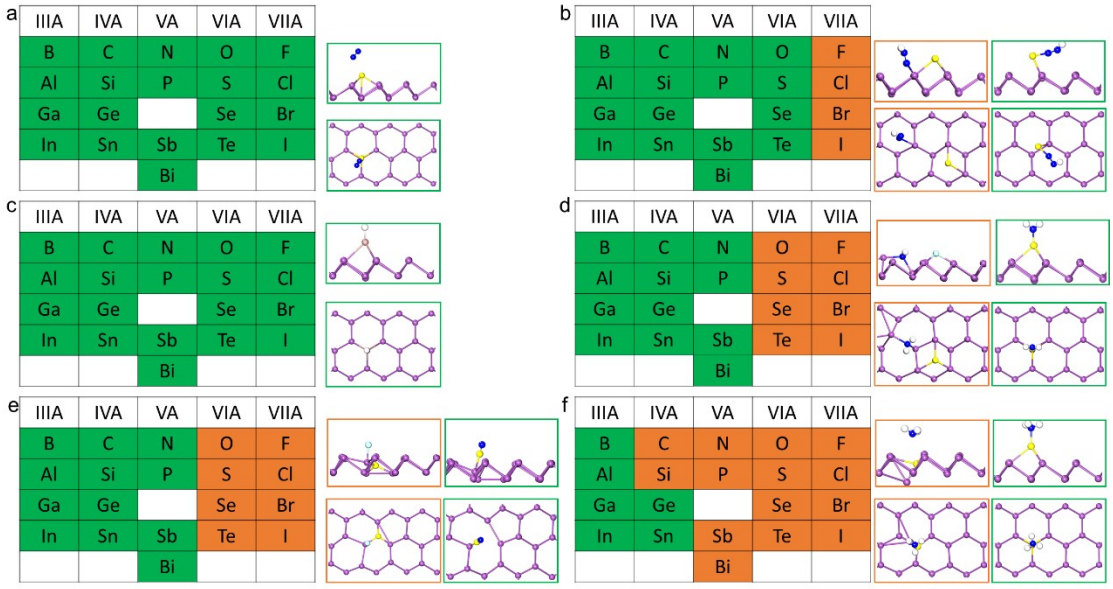

Figure S4 Optimized adsorption models of key intermediates N_2 (a), NNH (b), H (c), NH_2 (d), N (e), NH_3 (f) on the p-block element adsorbed onto bismuthine. Purple, yellow, blue, and white balls represent Bi, adsorbed p-block element, N and H atom, respectively. The orange and green colors represent the different adsorption configurations of key intermediates.

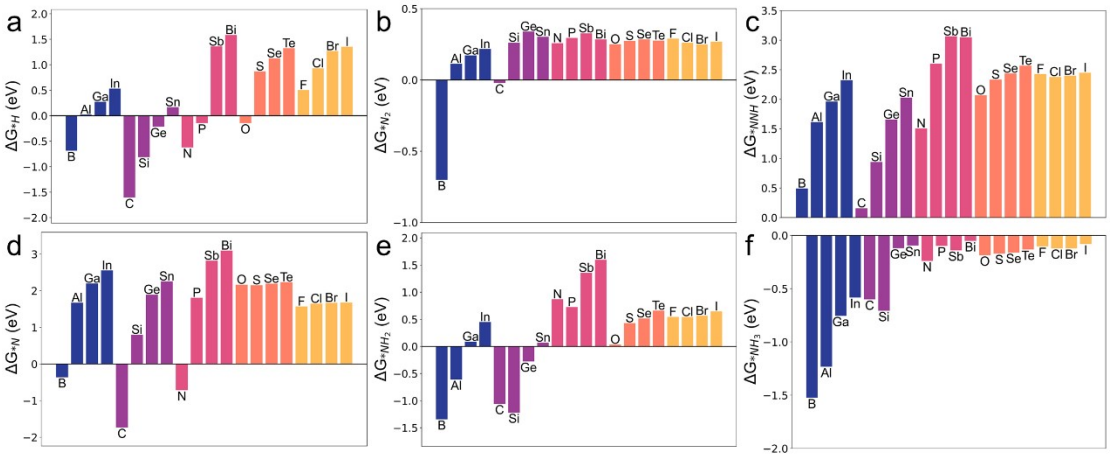

Figure S5 Adsorption energy of key NRR intermediates H (a), N_2 (b), NNH (c), N (d), NH_2 (e), NH_3 (f) on the *p*-block element doped into bismuthine.

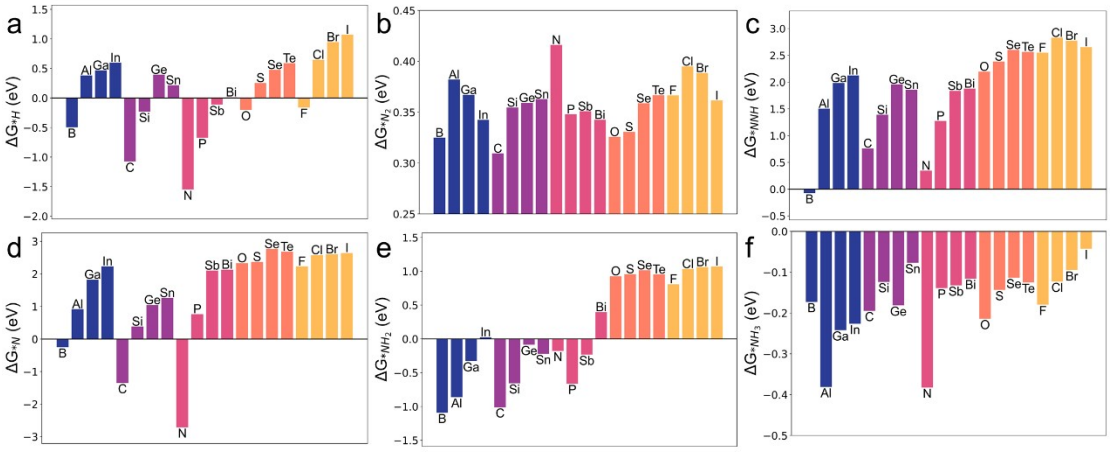

Figure S6 Adsorption energy of key NRR intermediates H (a), N_2 (b), NNH (c), N (d), NH_2 (e), NH_3 (f) on the *p*-block element adsorbed onto bismuthine.

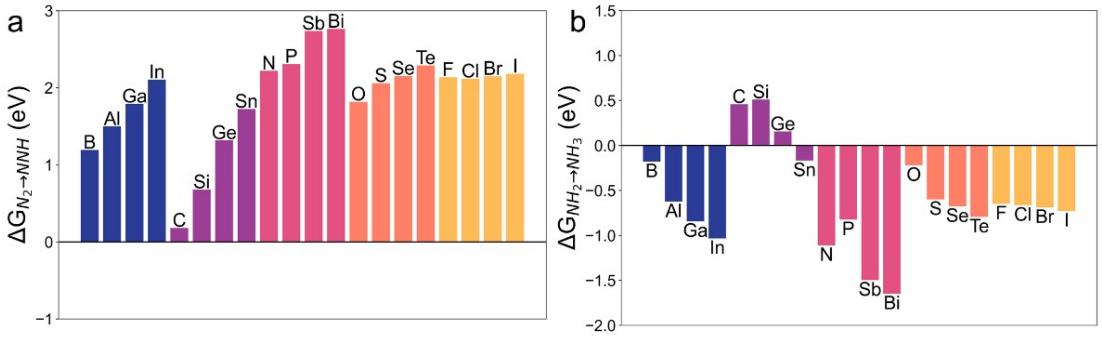

Figure S7 Reaction energy of *N_2 to *NNH (a) and *NH_2 to NH_3 (b) on the *p*-block element doped into bismuthine.

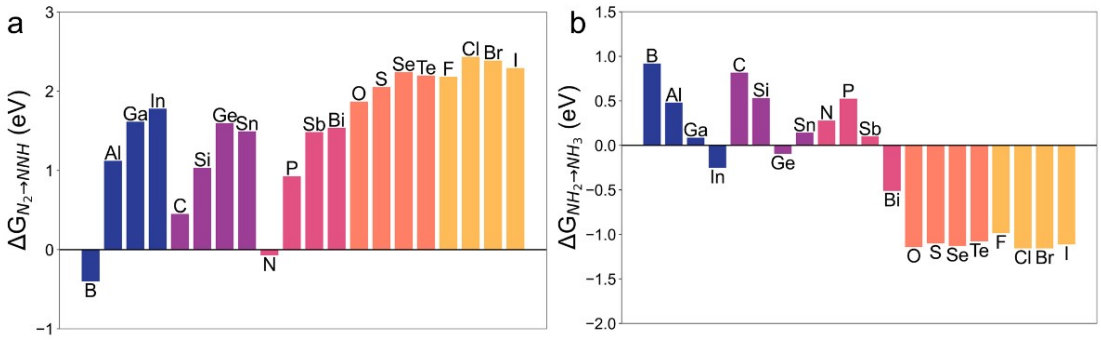

Figure S8 Reaction energy of *N_2 to *NNH (a) and *NH_2 to NH_3 (b) on the *p*-block element adsorbed onto bismuthine.

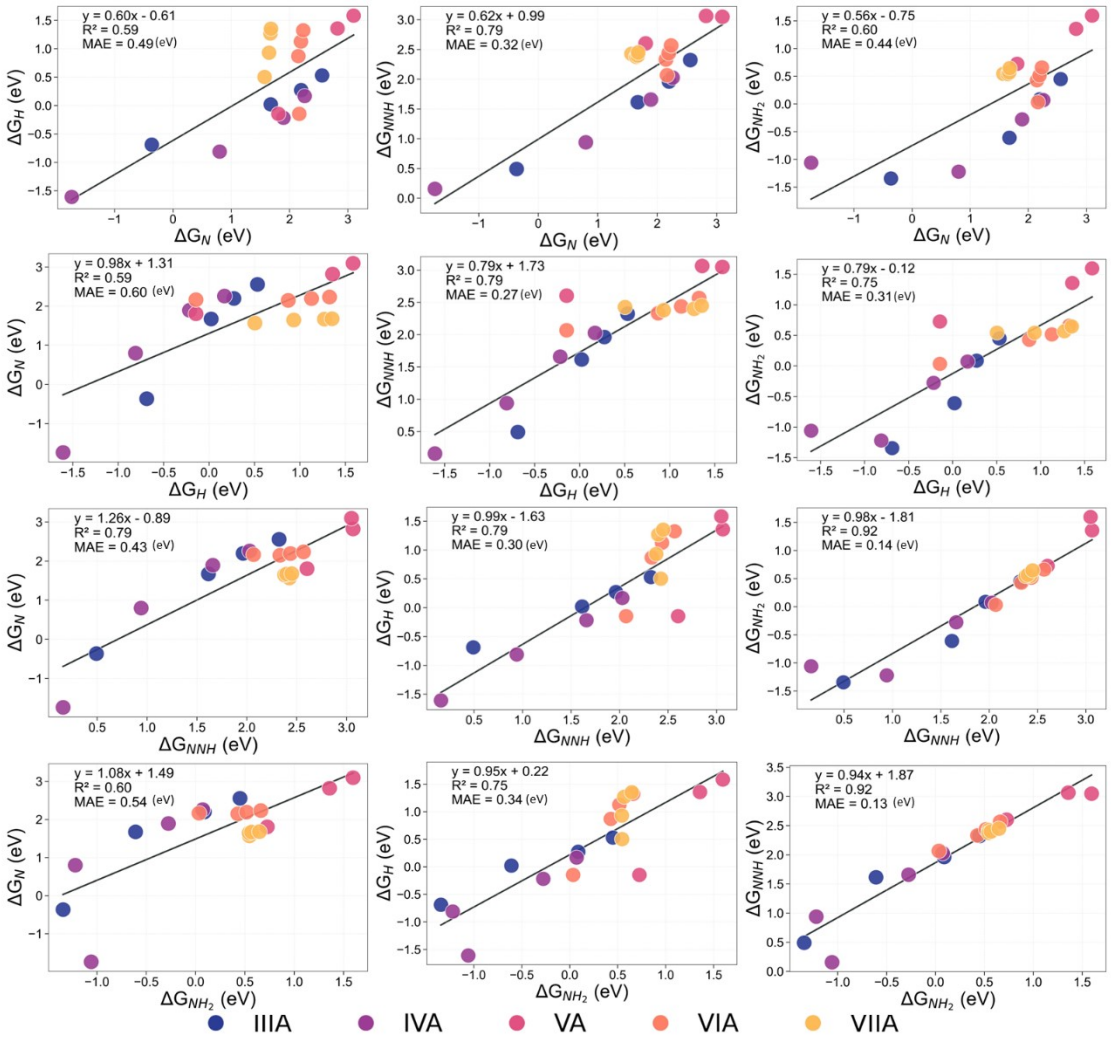

Figure S9 Scaling correlation between adsorption energies of different intermediates on the *p*-block element doped into bismuthine. In the legend, the five colored dots correspond to specific elemental groups: IIIA, IVA, VA, VIA, and VIIA. The color-coded dots indicate designated element groups, where dots sharing the same color represent elements belonging to the same main group.

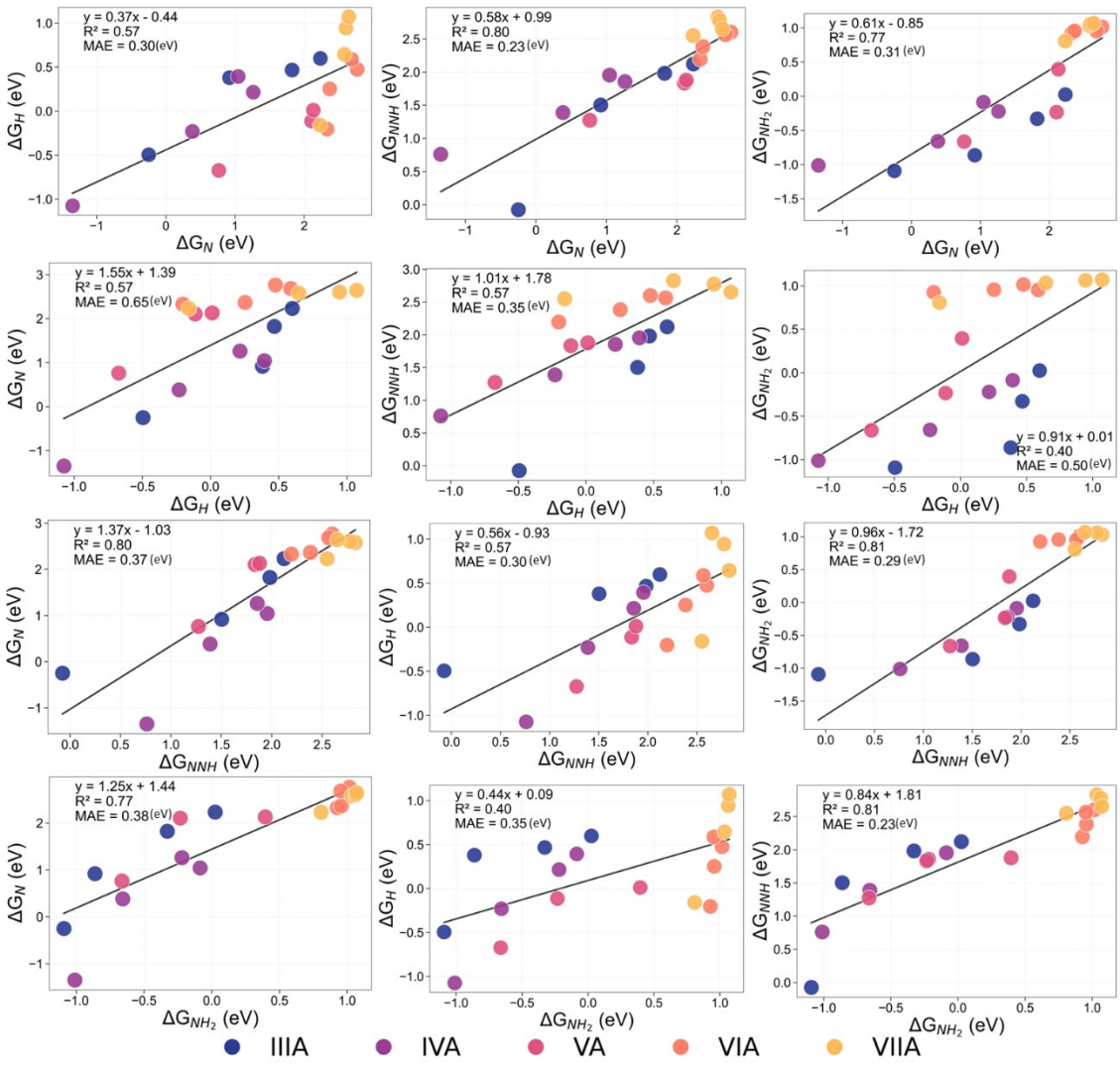

Figure S10 Scaling correlation between adsorption energies of different intermediates on the *p*-block element adsorbed onto bismuthine. In the legend, the five colored dots correspond to specific elemental groups: IIIA, IVA, VA, VIA, and VIIA. The color-coded dots indicate designated element groups, which dots sharing the same color represent elements belonging to the same main group.

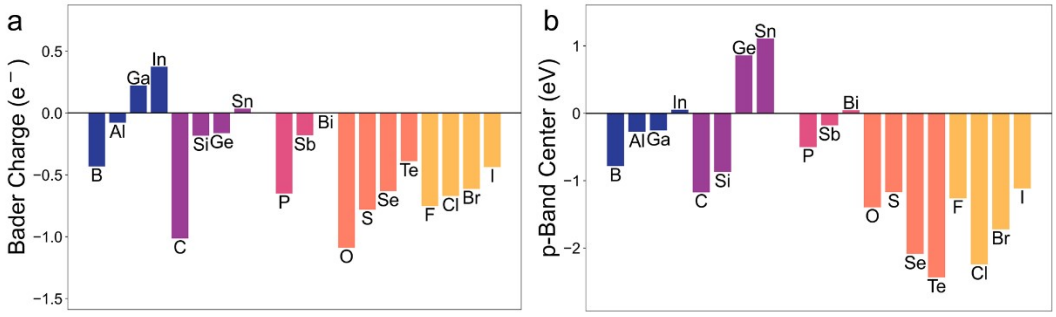

Figure S11 Bader charge (a) and p-band center (b) of doped *p*-block elements on the bismuthine.

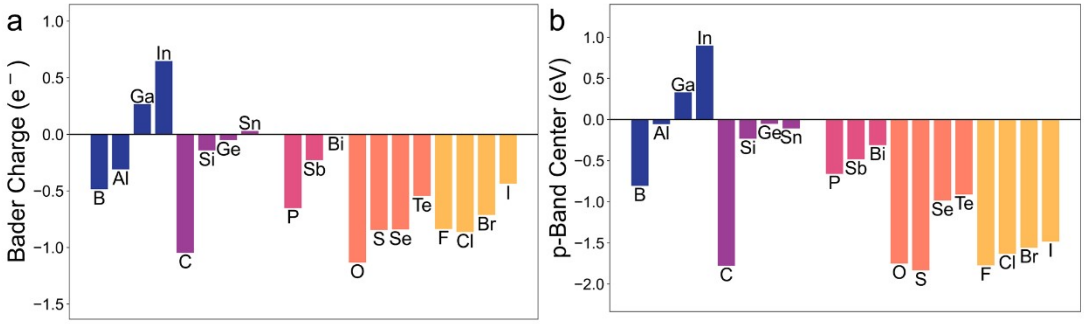

Figure S12 Bader charge (a) and p-band center (b) of adsorbed *p*-block elements on the bismuthine.

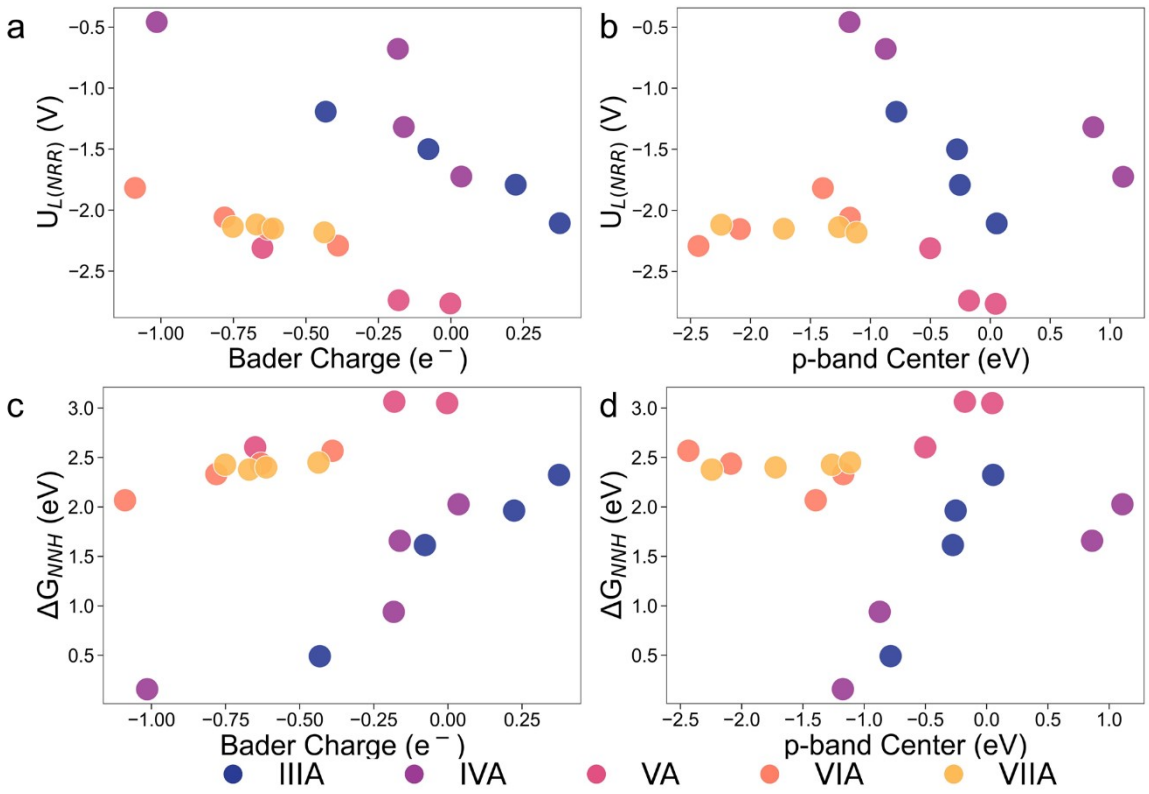

Figure S13 Scatter diagrams between U_L(NRR) (a, c), ΔG_{*NNH} (b, d) and Bader charge, *p*-band center on the *p*-block element doped into bismuthine. In the legend, the five colored dots correspond to specific elemental groups: IIIA, IVA, VA, VIA, and VIIA. The color-coded dots indicate designated element groups, which dots sharing the same color represent elements belonging to the same main group.

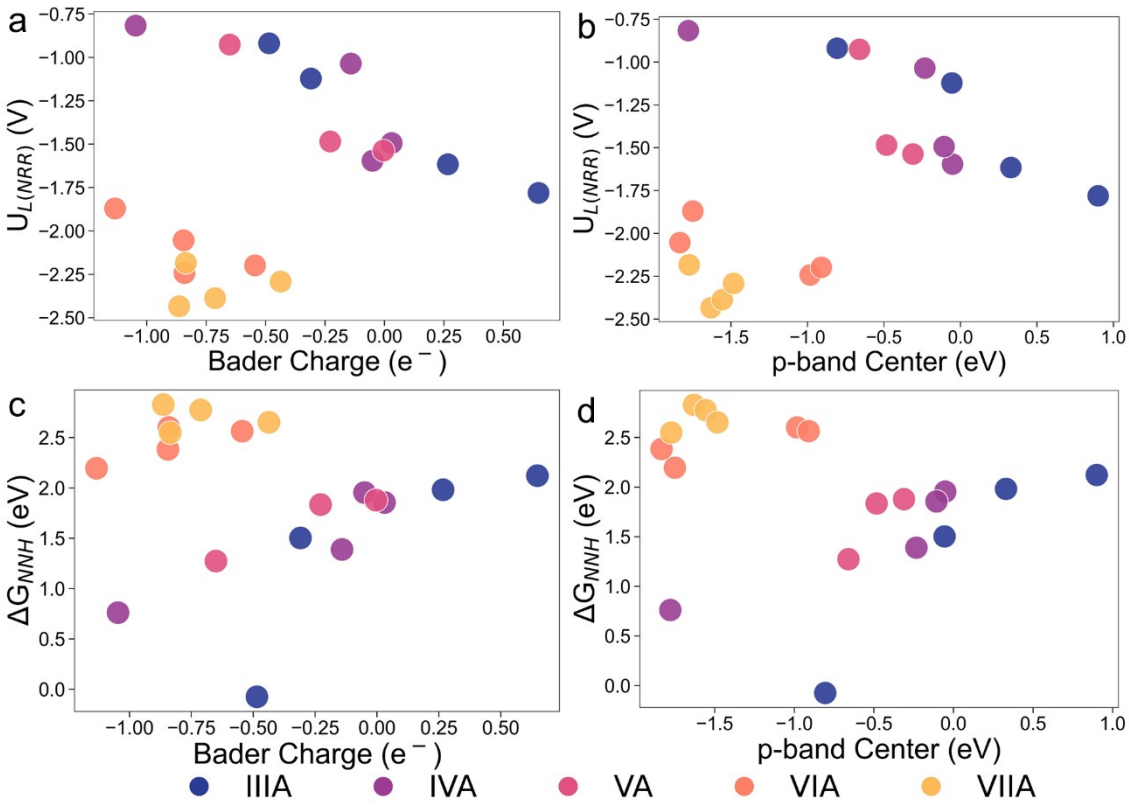

Figure S14 Scatter diagrams between U_L(NRR) (a, c), ΔG_{*NNH} (b, d) and Bader charge, *p*-band center on the *p*-block element doped into bismuthine. In the legend, the five colored dots correspond to specific elemental groups: IIIA, IVA, VA, VIA, and VIIA. The color-coded dots indicate designated element groups, which dots sharing the same color represent elements belonging to the same main group.

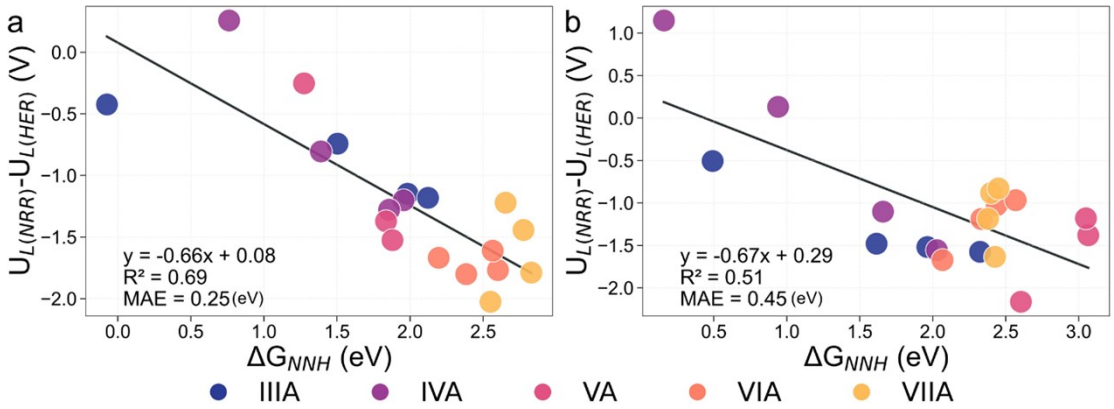

Figure S15 Scaling correlation between $U_L(NRR)-U_L(HER)$ and ΔG_{*NNH} on the doped (a) and adsorbed (b) into bismuthine. In the legend, the five colored dots correspond to specific elemental groups: IIIA, IVA, VA, VIA, and VIIA. The color-coded dots indicate designated element groups, which dots sharing the same color represent elements belonging to the same main group.

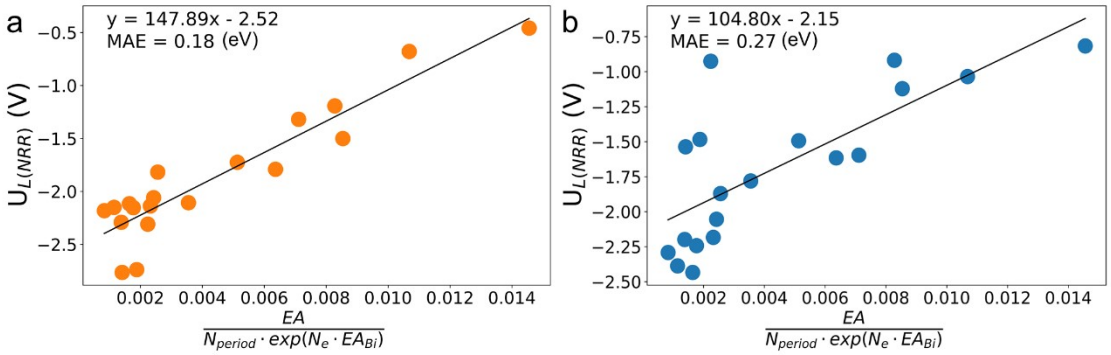

Figure S16 Scaling correlation between U_L(NRR) and 1D descriptor acquired by the SISSO algorithm on the bismuthine doped (a) and adsorbed (b) by p-block elements.

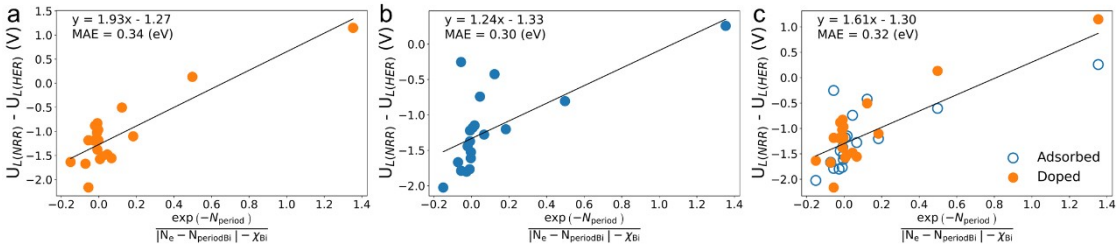

Figure S17 Scaling correlation between U_L(NRR)–U_L(HER) and 1D descriptor acquired by the SISSO algorithm on the bismuthine doped (a), adsorbed (b) and sum of doped and adsorbed (c) by p-block elements.

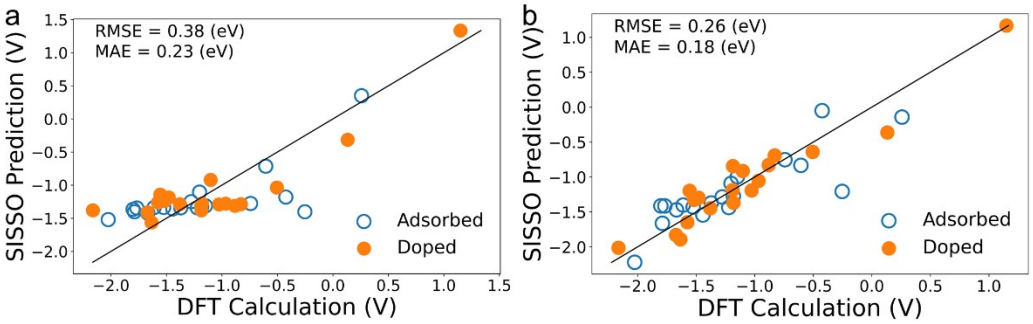

Figure S18 Fitting curve of U_L(NRR)–U_L(HER) between DFT calculation and SISSO prediction result by 1D (a) and 2D (b) descriptors.

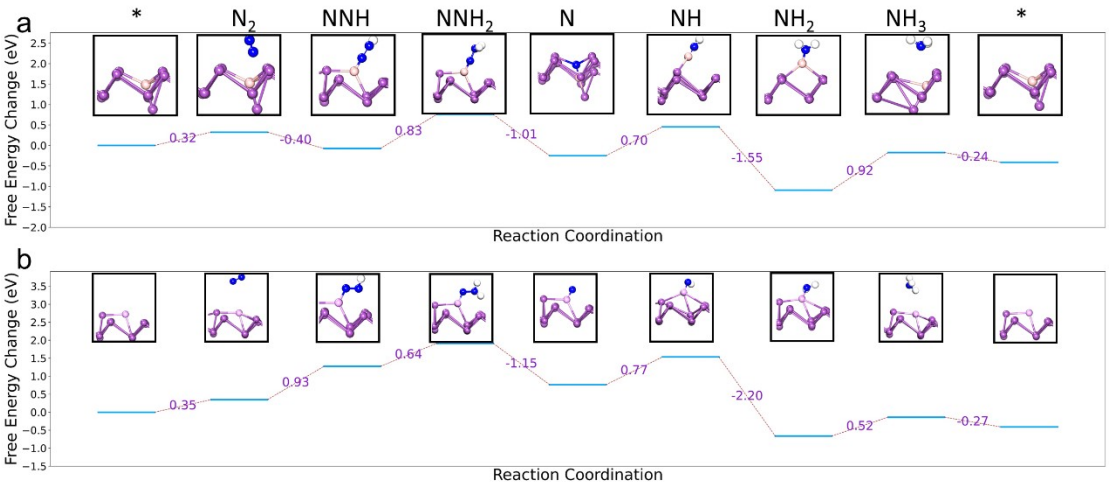

Figure S19 The free energy diagram of distal-associative pathway for NRR on the B- (a) and P- (b) adsorbed on bismuthine.

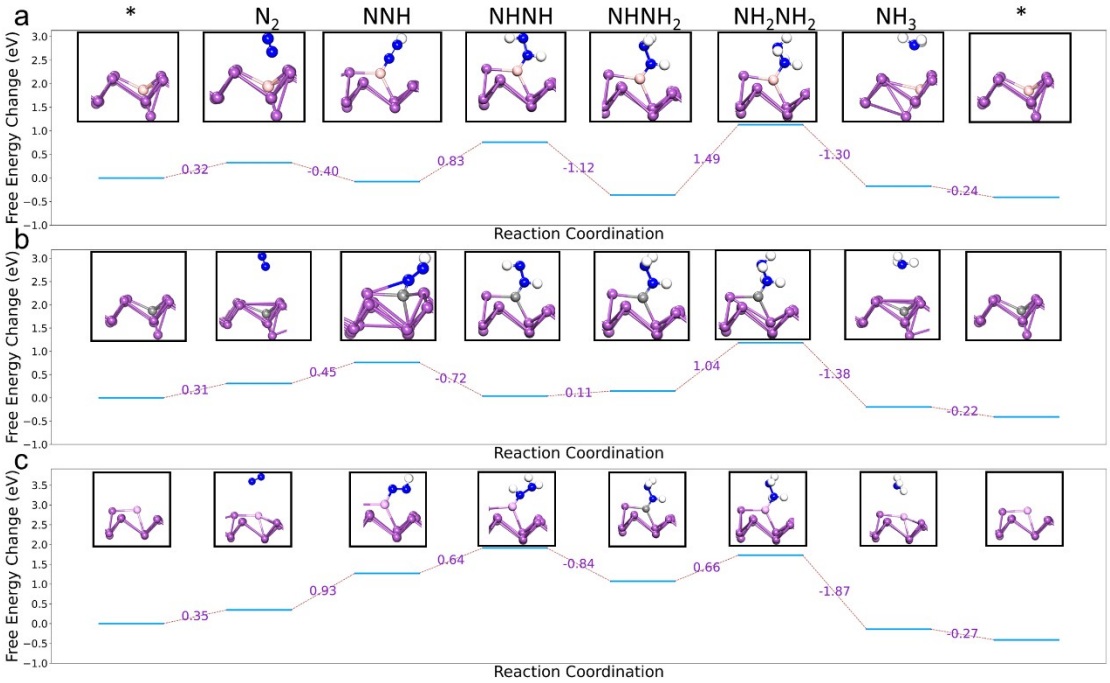

Figure S20 The free energy diagram of alternating-associative pathway for NRR on the B- (a), C- (b), and P-(c) adsorbed on bismuthine.

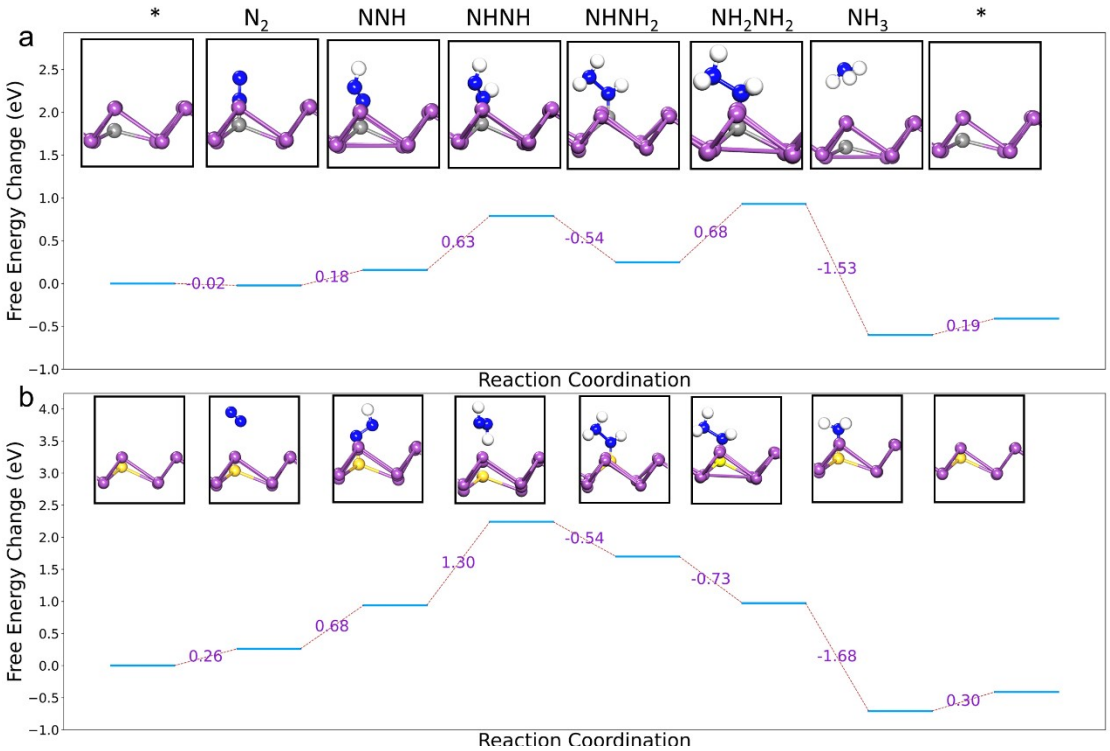

Figure S21 The free energy diagram of alternating-associative pathway for NRR on C- (a) and Si- (b) doped on bismuthine.

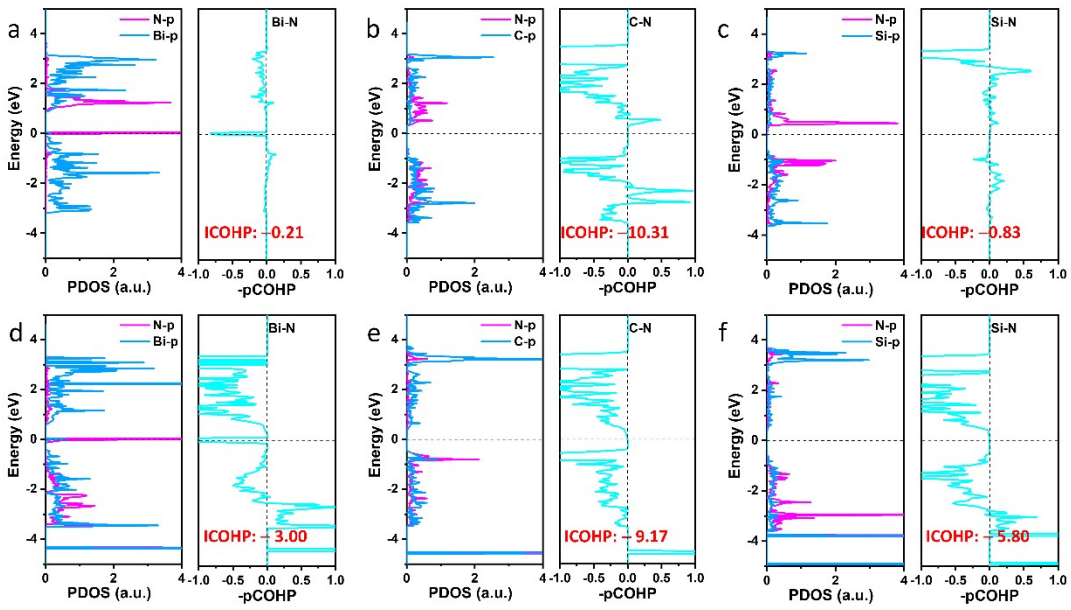

Figure S22 Partial density of state (left) and Crystal Overlap Hamilton Populations (right) of NNH and NH_2 intermediate on the pure bismuthine (a, d), C-doped Bi (b, e), and Si-doped Bi (c, f).

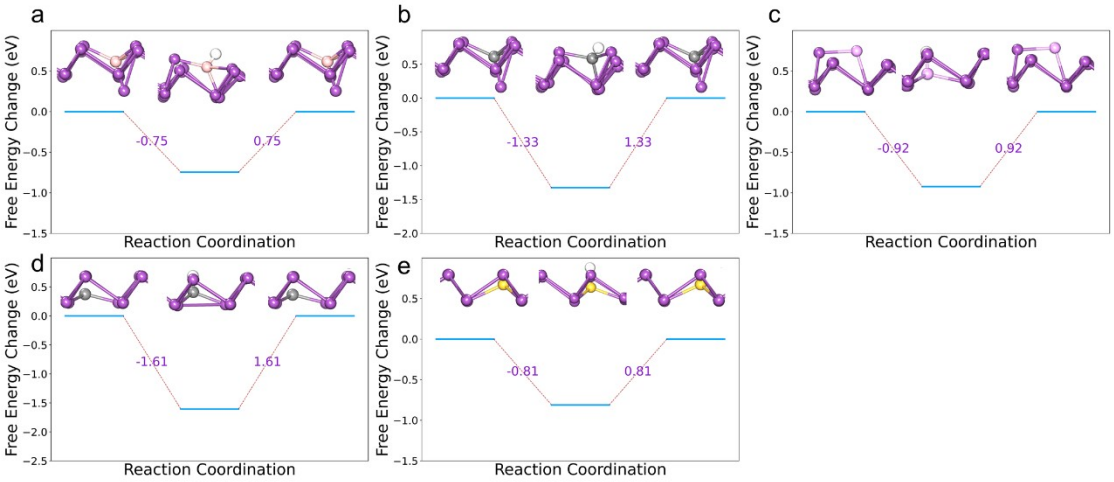

Figure S23 The free energy diagram for HER on B-(a), C- (b), P(c) adsorbed on and C-(d), Si-(e) doped on bismuthine.

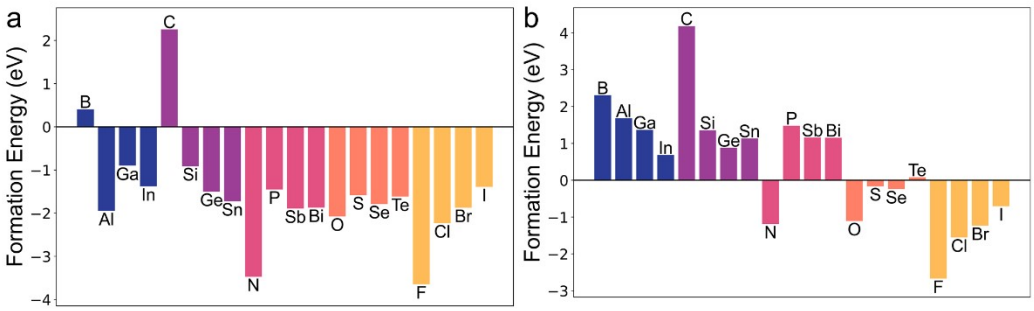

Figure S24 The formation energy diagram p-block element doped (a) and adsorbed (b) into bismuthine.

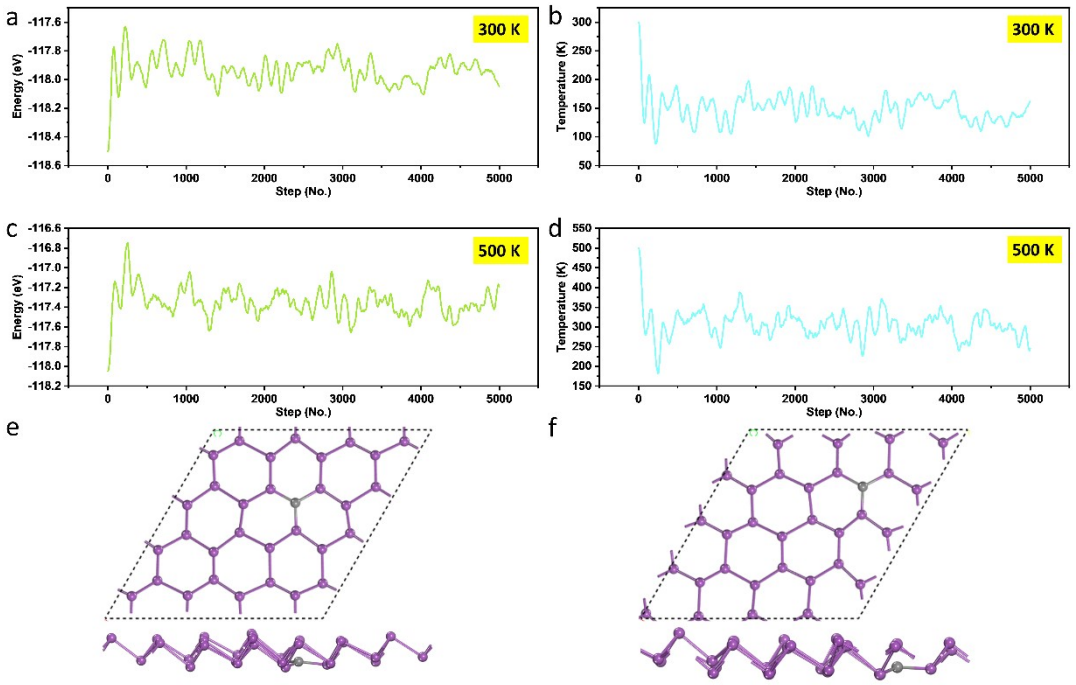

Figure S25 Molecular dynamics results about energy and temperature on the C-doped onto bismuthine under the 300 (a, b, e) and 500 K (c, d, f). Purple and gray ball represents Bi and C atom, respectively.

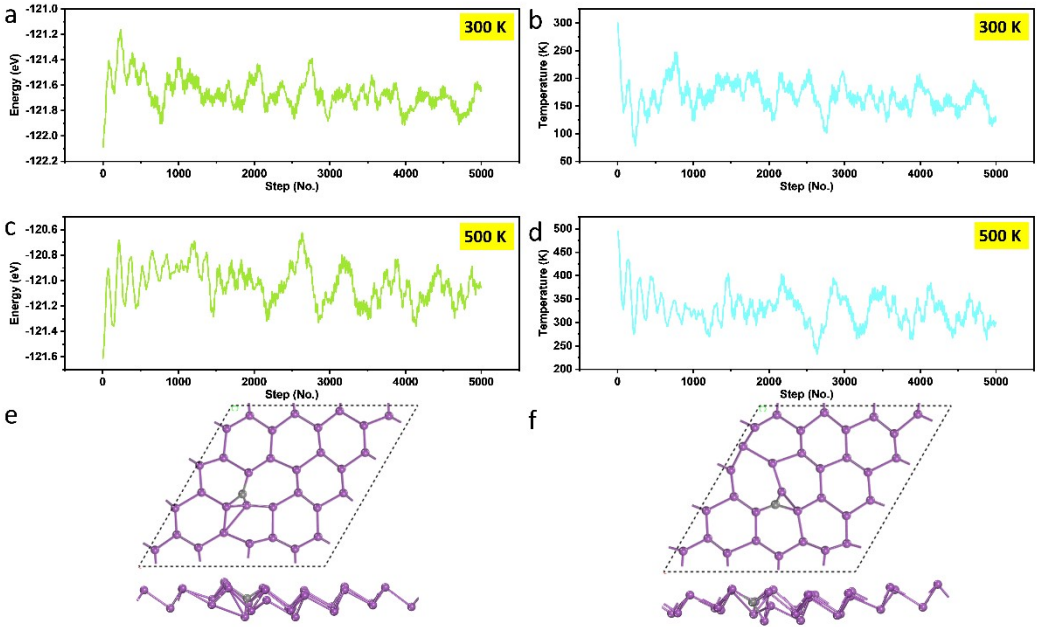

Figure S26 Molecular dynamics results about energy and temperature on the C-adsorbed onto bismuthine under the 300 (a, b, e) and 500 K (c, d, f). Purple and gray ball represents Bi and C atom, respectively.

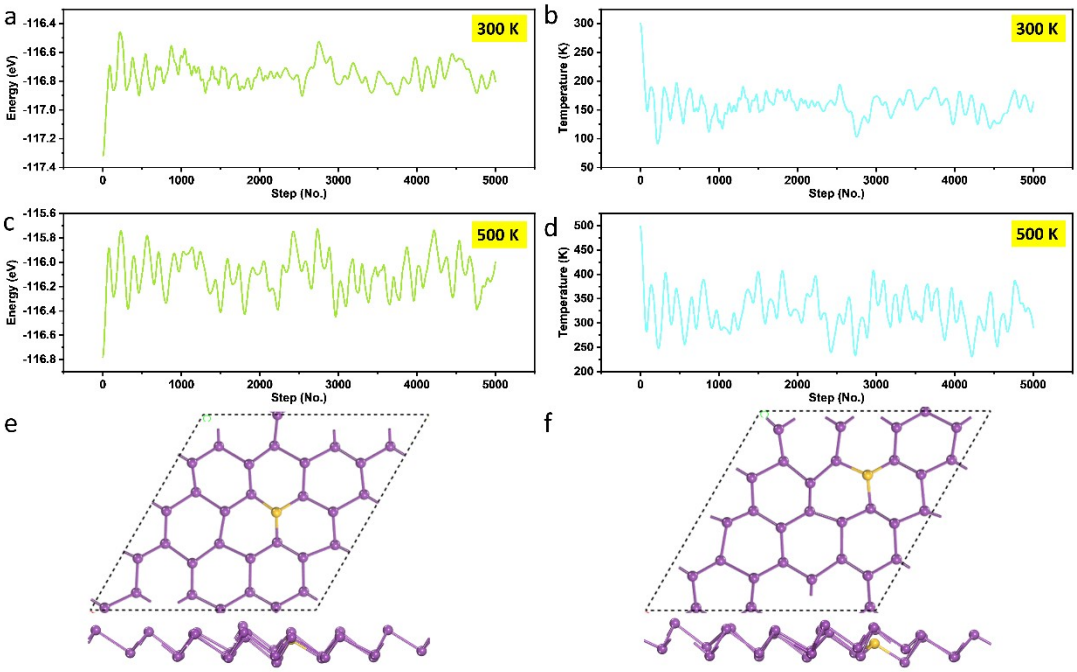

Figure S27 Molecular dynamics results about energy and temperature on the Si-doped onto bismuthine under the 300 (a, b, e) and 500 K (c, d, f). Purple and gray ball represents Bi and Si atom, respectively.

Section 3 Tables

Table S1 Adsorption energy of intermediates *N, *H, *N_2, *NNH, *NH_2, and *NH_3 on the p-block element doped into bismuthine.

Element	ΔG_N (eV)	ΔG_H (eV)	ΔG_{N2} (eV)	ΔG_{NNH} (eV)	ΔG_{NH2} (eV)	ΔG_{NH3} (eV)
B	-0.36	-0.69	-0.70	0.49	-1.34	-1.52
Al	1.67	0.02	0.11	1.61	-0.61	-1.23
Ga	2.20	0.27	0.17	1.96	0.09	-0.75
In	2.56	0.53	0.22	2.32	0.45	-0.58
C	-1.74	-1.61	-0.02	0.16	-1.06	-0.60
Si	0.80	-0.81	0.26	0.94	-1.22	-0.71
Ge	1.89	-0.22	0.34	1.66	-0.28	-0.12
Sn	2.26	0.17	0.30	2.03	0.07	-0.10
N	-0.71	-0.62	0.26	1.51	0.87	-0.24
P	1.81	-0.15	0.29	2.60	0.73	-0.10
Sb	2.82	1.36	0.33	3.06	1.36	-0.14
Bi	3.10	1.58	0.28	3.05	1.60	-0.05
O	2.17	-0.15	0.25	2.07	0.03	-0.19
S	2.15	0.87	0.27	2.33	0.43	-0.17
Se	2.19	1.13	0.28	2.44	0.52	-0.16
Te	2.23	1.32	0.28	2.57	0.66	-0.13
F	1.57	0.50	0.29	2.43	0.54	-0.10
Cl	1.65	0.93	0.26	2.38	0.54	-0.12
Br	1.67	1.27	0.25	2.40	0.57	-0.12
I	1.68	1.35	0.27	2.45	0.65	-0.08

Table S2 Adsorption energy of intermediates N, *H, $*N_2$, *NNH, $*NH_2$, and $*NH_3$ on the p-block atom adsorbed on bismuthine.

Element	ΔG_N (eV)	ΔG_H (eV)	ΔG_{N2} (eV)	ΔG_{NNH} (eV)	ΔG_{NH2} (eV)	ΔG_{NH3} (eV)
B	-0.25	-0.49	0.32	-0.07	-1.09	-0.17
Al	0.92	0.38	0.38	1.50	-0.86	-0.38
Ga	1.82	0.47	0.37	1.98	-0.33	-0.24
In	2.23	0.60	0.34	2.12	0.03	-0.23
C	-1.35	-1.07	0.31	0.76	-1.01	-0.19
Si	0.38	-0.23	0.35	1.39	-0.66	-0.12
Ge	1.04	0.39	0.36	1.96	-0.09	-0.18
Sn	1.26	0.22	0.36	1.86	-0.22	-0.08
N	-2.71	-1.55	0.42	0.35	-0.18	-0.38
P	0.76	-0.67	0.35	1.27	-0.66	-0.14
Sb	2.11	-0.11	0.35	1.83	-0.23	-0.13
Bi	2.13	0.01	0.34	1.88	0.40	-0.12
O	2.33	-0.20	0.33	2.20	0.93	-0.21
S	2.37	0.25	0.33	2.38	0.96	-0.14
Se	2.77	0.48	0.36	2.60	1.02	-0.11
Te	2.69	0.59	0.37	2.57	0.95	-0.13
F	2.23	-0.16	0.37	2.55	0.81	-0.18
Cl	2.58	0.65	0.39	2.83	1.03	-0.12
Br	2.61	0.94	0.39	2.78	1.06	-0.10
I	2.64	1.07	0.36	2.65	1.07	-0.04

Table S3 Primary features of p-block element and corresponding abbreviation and unit.

Name	Abbreviation	Unit
Pauling electronegativity	χ	dimensionless
Pauling electronegativity of Bi	χ_{Bi}	dimensionless
Valence electron number	N_e	dimensionless
Valence electron number of Bi	N_{eBi}	dimensionless
Periodic number	N_{period}	dimensionless
Periodic number of Bi	$N_{periodBi}$	dimensionless
Group number	N_{group}	dimensionless
Mendeleev number	M_{men}	dimensionless
Atomic number	N_{atom}	dimensionless
Number of electron layers	N_{es}	dimensionless
Electron affinity	EA	eV
Electron affinity of Bi	EA_{Bi}	eV
Covalent radius	R_{atom}	Å
Covalent radius of Bi	R_{atomBi}	Å
Ionization Energy	IE	eV

Table S4 The basic attributes of the element including occupied valence electron number (N_e), periodic number (N_{period}), covalent radius (R_{atom}), electronegativity (χ), electron affinity (EA), Group number (N_{group}), Mendeleev number (M_{men}), Number of electron layers (N_{es}) and Ionization Energy (IE).

element	χ	N_e	N_{period}	EA	R_{atom}	N_{group}	M_{men}	N_{es}	IE
B	2.04	3	2	0.28	0.85	13	81	2	8.30
Al	1.61	3	3	0.43	1.25	13	82	3	5.99
Ga	1.81	3	4	0.43	1.30	13	83	4	6.00
In	1.78	3	5	0.30	1.55	13	84	5	5.79
C	2.55	4	2	1.26	0.70	14	87	2	11.26
Si	1.90	4	3	1.39	1.10	14	88	3	8.15
Ge	2.01	4	4	1.23	1.25	14	89	4	7.90
Sn	1.96	4	5	1.11	1.45	14	90	5	7.34
N	3.04	5	2	0.07	0.65	15	93	2	14.53
P	2.19	5	3	0.75	1.00	15	94	3	10.49
Sb	2.05	5	5	1.05	1.45	15	96	5	8.64
Bi	1.90	5	6	0.94	1.60	15	97	6	7.29
O	3.44	6	2	1.46	0.60	16	99	2	13.62
S	2.58	6	3	2.08	1.00	16	100	3	10.36
Se	2.55	6	4	2.02	1.15	16	101	4	9.75
Te	2.10	6	5	1.97	1.40	16	102	5	9.01
F	3.98	7	2	3.40	0.50	17	106	2	17.42
Cl	3.16	7	3	3.61	1.00	17	107	3	12.97
Br	2.96	7	4	3.36	1.15	17	108	4	11.81
I	2.66	7	5	3.06	1.40	17	109	5	10.45

Table S5 The descriptor of target U_L(NRR) with lowest RMSE for each dimension, complexity and task. χ, N_e, N_{period}, EA, R_{atom}, χ_{Bi}, N_{eBi}, $N_{periodBi}$, EA_{Bi}, R_{atomBi} indicates electronegativity, Valence electron number, Periodic number, Electron affinity, covalent radius and these feature of Bi.

Dimension	Complexity	Descriptor	Task	Coefficient	Intercept	RMSE	MaxAE
1	1	$N_e + N_{period}$	1	-0.21	0.16	0.37	0.79
			2	-0.24	0.18		
2	1	$\sqrt[3]{Ne}$	1	-3.56	4.66	0.31	0.81
				-0.77			
		$\frac{N_{period}}{EA}$	2	-4.27	5.99		
				-0.15			
3	1	N_e^3	1	-0.01	-0.10	0.21	0.65
				0.13			
		$EA*^{R_{atom}}$		-0.72			
				-0.01			
		$\log(^{R_{atom}})$	2	0.98	-1.38		
				-2.60			
1	2	$\frac{N_{eBi} - \chi}{Ratom}$	1	0.84	-3.66	0.35	0.84
			2	0.88	-3.95		
2	2	$\frac{N_e - N_{periodBi}}{R_{atom}}$	1	-0.36	-2.35	0.24	0.55
				0.50			
		$\sqrt[3]{\frac{EA}{N_{period}}}$	2	-0.59	-4.63		
				3.10			
3	2	$\frac{1}{\exp(EA) \cdot R_{atom}}$	1	2.86	-5.28	0.15	0.32
				1.08			
		$\frac{1}{\exp(\lvert N_e - N_{eBi} \rvert)}$		102.62			
				2.92			
		$\sqrt[3]{\frac{EA}{N_e}}$	2	0.07	-6.91		
				180.33			
1	3	$\frac{EA}{N_{period} \cdot \exp(N_e)}$	1	128.75	-2.13	0.29	0.99
			2	177.58	-2.49		
2	3	$\frac{EA}{N_e^3 \cdot N_{period}}$	1	187.65	-3.13	0.19	0.57
				1.23			
		$\frac{N_e - \chi}{\exp(EA)}$	2	263.17	-2.87		
				0.04			

1	4	$\frac{EA}{N_{period} \cdot \exp(N_e \cdot EA_{Bi})}$	1	104.80	-2.15	0.29	0.98
			2	147.89	-2.52		
2	4	$\frac{1}{\exp(\lvert EA - EA_{Bi}\rvert) \cdot \chi \cdot N_{period}}$	1	118.07 -1.42	-2.49	0.14	0.36
		$\frac{N_e}{\lvert EA - EA_{Bi}\rvert + EA}$	2	174.14 -0.53	-1.67		

Table S6 The descriptor of U_L(NRR)-U_L(HER) with lowest RMSE for each dimension, complexity and task. χ, N_e, N_{period}, EA, R_{atom}, χ_{Bi}, N_{eBi}, $N_{periodBi}$, EA_{Bi}, R_{atomBi} indicates electronegativity, Valence electron number, Periodic number, Electron affinity, covalent radius and these feature of Bi.

Dimension	Complexity	Descriptor	Task	Coefficient	Intercept	RMSE	MaxAE
1	1	$\frac{N_{period}}{R_{atom}}$	1	-0.90	1.68	0.56	2.04
			2	-0.53	0.61		
2	1	$\frac{\chi}{R_{atom}}$	1	-1.02 4.53	-3.08	0.49	1.51
		$\frac{1}{R_{atom}}$	2	-0.69 3.31	-2.58		
3	1	$\sqrt[3]{EA}$	1	0.93 -0.48	-2.85	0.33	1.05
		$\frac{N_e}{R_{atom}}$	2	3.11 4.24	-6.63		
		$\frac{1}{R_{atom}}$		-0.88 5.45			
1	2	$\frac{N_e - \chi}{R_{atom}}$	1	0.88	-3.29	0.51	1.48
			2	0.66	-2.63		
2	2	$\frac{N_e - N_{periodBi}}{R_{atom}}$	1	-0.55 0.59	-2.79	0.33	0.62
		$\sqrt[3]{EA - N_e}$	2	-1.05 2.18	-6.11		
3	2	$\frac{N_{eBi} - \chi}{R_{atom}}$	1	1.11 -0.92	-2.65	0.26	0.74
		$\exp(\frac{N_{period}}{EA})$		0.05			

						1.88				
	N_2	NNH	NHNH	NNH_2	$NHNH_2$	2 NH_2NH_2	N	1.28 NH	NH_2	NH_3
C doped	-0.02	0.16	0.79	-0.14	0.25	0.93	-1.02	-1.00	-1.06	-0.60
Si doped	0.26	0.94	2.24	0.88	1.70	0.97	0.80	0.09	-1.22	-0.71
B adsorbed	0.32	-0.07	0.76	0.76	-0.36	1.13	-0.25	0.45	-1.09	-0.17
C adsorbed	0.31	0.76	0.04	0.04	0.15	1.19	-1.35	-0.68	-1.01	-0.19
P adsorbed	0.35	1.27	1.91	1.91	1.07	1.73	0.76	1.53	-0.66	-0.14
			$N_e \cdot (N_{period} - N_{periodBi})$				-7.04			
							0.19			
1	3		$\frac{\mathrm{EA}}{\mathrm{N_{period}} \cdot \mathrm{N_e}}$		1	140.90	-1.70		0.46	1.01
					2	151.25	-1.61			
2	3		$\frac{\mathrm{N_e} - \mathrm{N_{periodBi}}}{\mathrm{N_{period}}^2}$		1	-2.42	-1.37		0.30	1.01
						-1.61				
			$\frac{\exp(-EA)}{(\mathrm{N_{period}} + \chi_{\mathrm{Bi}})}$		2	-5.55	-0.44			
						-21.02				
1	4		$\frac{\exp(-\mathrm{N_{period}})}{\lvert\mathrm{N_e} - \mathrm{N_{periodBi}}\rvert - \chi_{\mathrm{Bi}}}$		1	1.24	-1.33		0.38	1.14
					2	1.93	-1.27			
			$\frac{(N_e - N_{periodBi}) \cdot (N_{period} - N_{periodl}}{R_{atom}}$		1	0.12	-1.14			
						-2.64				
2	4		$\frac{\exp(-\frac{EA}{\mathrm{N_{period}}})}{(\mathrm{N_{period}} + \chi_{\mathrm{Bi}})}$		2	0.29	1.89		0.26	0.95
						-30.10				

Table S7 The free energy change of elementary steps for NRR on the potential candidates.

Table S8 The adsorption energy of key intermediates on the doped-Bi using the test results of 400eV and 500eV cut-off energy.

	N_2	NNH	NH_2	NH_3	$\Delta G_{N2\rightarrow NNH}$	$\Delta G_{NH2\rightarrow NH3}$
C_500eV	-0.03	0.23	-1.07	-0.61	0.26	0.45
Si_500eV	0.23	0.94	-1.28	-0.73	0.71	0.55
C_400eV	-0.02	0.16	-1.06	-0.6	0.18	0.46
Si_400eV	0.26	0.94	-1.22	-0.71	0.68	0.51

Note: the effect of cutoff energy on the adsorption energy of intermediates are very small, all less than 0.1 eV within DFT error, that can be neglected.

References

1. Zhi, C.; Cai, S.; Sun, D.; Yang, J.; Sun, Z., A Simple Descriptor toward Optimizing Electrocatalytic N2 Oxidation to HNO3 Performance over Graphene-Based Single-Atom Catalysts. *J. Phys. Chem. Lett.* **2025,** *16* (11), 2742-2751.
2. Hammer, B.; Hansen, L. B.; Nørskov, J. K., Improved adsorption energetics within density-functional theory using revised Perdew-Burke-Ernzerhof functionals. *Phys. Rev. B* **1999,** *59* (11), 7413-7421.
3. Perdew, J. P.; Burke, K.; Ernzerhof, M., Generalized Gradient Approximation Made Simple. *Phys. Rev. Lett.* **1996,** *77*, 3865-3868.
4. Grimme, S.; Antony, J.; Ehrlich, S.; Krieg, H., A consistent and accurate ab initio parametrization of density functional dispersion correction (DFT-D) for the 94 elements H-Pu. *J. Chem. Phys.* **2010,** *132* (15), 154104.
5. Mathew, K.; Sundararaman, R.; Letchworth-Weaver, K.; Arias, T. A.; Hennig, R. G., Implicit solvation model for density-functional study of nanocrystal surfaces and reaction pathways. *J. Chem. Phys.* **2014,** *140*, 084106.
6. Maintz, S.; Deringer, V. L.; Tchougreeff, A. L.; Dronskowski, R., LOBSTER: A tool to extract chemical bonding from plane-wave based DFT. *J. Comput. Chem.* **2016,** *37* (11), 1030-5.
7. Wang, V.; Xu, N.; Liu, J.-C.; Tang, G.; Geng, W.-T., VASPKIT: A user-friendly interface facilitating high-throughput computing and analysis using VASP code. *Comput. Phys. Commun.* **2021,** *267*, 108033.
8. Nørskov, J. K.; Rossmeisl, J.; Logadottir, A.; Lindqvist, L.; Kitchin, J. R.; Bligaard, T.; Jónsson, H., Origin of the Overpotential for Oxygen Reduction at a Fuel-Cell Cathode. *J. Phys. Chem. B* **2004,** *108*, 17886-17892.
9. Bucher, D.; Pierce, L. C.; McCammon, J. A.; Markwick, P. R., On the Use of Accelerated Molecular Dynamics to Enhance Configurational Sampling in Ab Initio Simulations. *J. Chem. Theory Comput.* **2011,** *7*, 890-897.
10. Wang, J.; Xie, H.; Wang, Y.; Ouyang, R., Distilling Accurate Descriptors from Multi-Source Experimental Data for Discovering Highly Active Perovskite OER Catalysts. *J. Am. Chem. Soc.* **2023,** *145* (20), 11457-11465.
11. Ouyang, R.; Curtarolo, S.; Ahmetcik, E.; Scheffler, M.; Ghiringhelli, L. M., SISSO: A compressed-sensing method for identifying the best low-dimensional descriptor in an immensity of offered candidates. *Phys. Rev. Mater.* **2018,** *2* (8), 083802.